On the Potential of Empirical Mode Decomposition for RFI Mitigation in Microwave Radiometry

Raúl Díez-García , *Graduate Student Member, IEEE*, Adriano Camps , *Fellow, IEEE*, and Hyuk Park , *Senior Member, IEEE*

***Abstract*— Radio-frequency interference (RFI) is an increasing problem particularly for Earth observation using microwave radiometry. RFI has been observed, for example, at L-band by the European Space Agency's (ESA's) soil moisture and ocean salinity (SMOS) Earth Explorer and by National Aero- nautics and Space Administration's (NASA's) soil moisture activepassive (SMAP) and Aquarius missions, as well as at C-band by Advanced Microwave Scanning Radiometer (AMSR)-E and AMSR-2, and at 10.7 and 18.7 GHz by AMSR-E, AMSR-2, WindSat, and GPM Microwave Imager (GMI). Therefore, systems dedicated to interference detection and removal of contaminated measurements are nowadays a must in order to improve radiometric accuracy and reduce the loss of spatial coverage caused by interference. In this work, the feasibility of using the empirical mode decomposition (EMD) technique for RFI mitigation is explored. The EMD, also known as Hilbert–Huang transform (HHT), is an algorithm that decomposes the signal into intrinsic mode functions (IMFs). The achieved performance is analyzed, and the opportunities and caveats that this type of methods present are described. EMD is found to be a practical RFI mitigation method, albeit presenting some limitations and considerable complexity. Nevertheless, in some conditions, EMD exhibits a better performance than other commonly used methods (such as frequency binning). In particular, it has been found that EMD performs well for RFI affecting the <25% lower part of the intermediate frequency (IF) bandwidth.**

***Index Terms*— Hilbert–Huang transform (HHT), interference, microwave radiometer, passive microwave remote sensing, radio-frequency interference (RFI), RFI detection.**

I. Introduction

MICROWAVE radiometers are increasingly affected by radio-frequency interference (RFI) [1], [2]. The presence of man-made signals, usually of much larger power than the natural emission itself, affects the radiometric resolution of the measurements making it difficult to achieve the high values required by many applications. These interferences conceal the underlying natural signal, corrupting, and even preventing the retrieval of geophysical variables. Passive remote-sensing bands are protected by the International Telecommunications Union (ITU) Radio Regulations, and considerable effort is devoted to enforce proper spectrum usage [3]. Nevertheless, RFI remains a considerable threat to the accuracy and spatial coverage of microwave passive instruments. The adoption of detection and mitigation techniques is then required to reduce the impact of RFI, increasing the radiometric accuracy and data reliability and extending the coverage to areas where measurements are normally lost due to interference. Over the last years, a wide range of RFI detection techniques has been developed. Some examples include:

1) parametric techniques, where the RFI type is known *a priori* [4];
2) statistical detection methods, where the statistics of the received signal are estimated and compared to the Gaussian ones, for example, [5], [6];
3) correlation-based detection methods, where the distortion on correlation can be used to detect RFI [7];
4) polarimetric methods, where the cross-polarization components may indicate the presence of RFI [8]; and
5) time and/or frequency analysis, where the time/frequency properties of the signal are studied to infer the presence of RFI [9].

In this work, and for the first time to the authors' knowledge, the suitability of the empirical mode decomposition (EMD) for RFI mitigation is explored. The EMD, also known asHilbert–Huang transform (HHT), decomposes the signal into several intrinsic mode functions (IMFs). The EMD can be interpreted as a nonlinear time–frequency decomposition tool, especially tailored for nonstationary signals. In this work, the EMD is evaluated as a potential RFI-mitigation tool and represents a first step toward the adoption of nonlinear decomposition methods.

II. Empirical Mode Decomposition

EMD is a useful algorithm for the decomposition of multiple-component signals into a set of the so-called IMF. In some cases, the resulting IMFs may approximate the original additive components of the signal, which often allowsfor useful interpretations of the physical origin of its parts. This property has made the EMD a useful algorithm for signal decomposition in several areas, such as biomedical analysis [10], seismic studies [11], or structural analysis [12].

The signal into consideration can be decomposed as

$$x(t) = \sum_i \mathrm{IMF}_i(t) + d(t) \tag{1}$$

where IMF_i is the i th "intrinsic mode function" resulting from the decomposition, and $d(t)$ is a remainder. The computation of each IMF is obtained by a process called "shifting" that can be summarized as follows [13, p. 917].

Manuscript received 27 January 2022; revised 2 May 2022; accepted 29 June 2022. Date of publication 4 July 2022; date of current version 19 July 2022. This work was supported in part by the Sensing With Pioneer- ing Opportunistic Techniques (SPOT) under Grant RTI2018-099008-B-C21/ AEI/10.13039/501100011033, in part by the RYC-2016-20918 under Grant MCIN/AEI/10.13039/501100011033, and in part by the European Social Fund (ESF), Investing in your future. *(Corresponding author: Raúl Díez-García.)*

The authors are with the Department of Signal Theory and Communications, Universitat Politecnica de Catalunya–BarcelonaTech, IEEC/CTE-UPC, 08034 Barcelona, Spain (e-mail: raul.diez@upc.edu; adriano.jose.camps@upc.edu; park.hyuk@upc.edu).

Digital Object Identifier 10.1109/TGRS.2022.3188171

1) Identify the local minima and maxima of the function $x(t)$.
2) With the help of an spline interpolator, create the upper and lower envelopes of $x(t)$ along the identified minima and maxima.
3) Compute the mean of the two envelopes: $m^1(t)$.
4) Subtract $m^1(t)$ from the original signal $x(t)$, obtain- ing a preliminary estimation of the first IMF, $h^1(t)$ $x(t)$ $m^1(t).=$ −
5) Proceed then to obtain a refined version of the IMF estimation, $h^2(t)$, by repeating steps 1–4 with $h^1(t)$ in the place of $x(t)$. Stop the shifting process once $m^n(t)$ falls below an arbitrary threshold for all t.

The described process allows to compute the first IMF. Subsequent IMFs can be obtained by recursively repeating the steps above on the residual signal d^i , obtained by subtracting the previous IMF to the original signal

$$d^i(t) = x(t) - \sum^{(i-1)} \text{IMF}. \tag{2}$$

IMFs are functions that have near-zero mean, positive maxima, and negative minima. Therefore, they resemble sinusoids that are modulated in frequency and amplitude. In Fig. 1, a signal composed by the addition of a sinusoid with a chirpis shown. As an example of the EMD capabilities, the result of the EMD decomposition is shown in Fig. 2. As it can be appreciated, EMD is capable of approximately untangling both signals without any *a priori* information on the frequency contents of its constituents. This makes EMD an adaptive, data-driven, nonparametric method for signal decomposition, able to separate even nonstationary signals. It can also be understood as a nonlinear time–frequency representation of the original signal.

Note that, in general, IMFs are not uncorrelated. In some conditions, EMD results in components that do not have physical meaning, thus hindering the effective use of EMD. This phenomenon is called "mode mixing," and it is described in [14]. It occurs when the constituent signals do share the same instantaneous frequency, or by the presence of pulsed bursts in the signal. To overcome this, several alternatives and refinements to EMD exist, such as, for example, the ensemble empirical mode decomposition (EEMD) [15], tai- lored to decompose pulsed signals. In addition, EMD or its variations remain mainly empirical methods, and their analytical foundations are still lacking [16].

III. Application of EMD to RFI Filtering

By construction, higher-order IMFs will exhibit larger-scale (i.e., slower) fluctuations. Therefore, the frequency contents will be lower in higher-order IMFs, with the first IMFs containing most of the high-frequency energy of the signal. This property makes the EMD a suitable technique for signal denoising, as initially identified by Huang *et al.* [13, p. 978]. Signal denoising with EMD is based on the determination ifa certain IMF contains useful signal energy or only noise. Once this has been determined for all IMFs, a denoised reconstructed signal can be computed by adding up only the useful

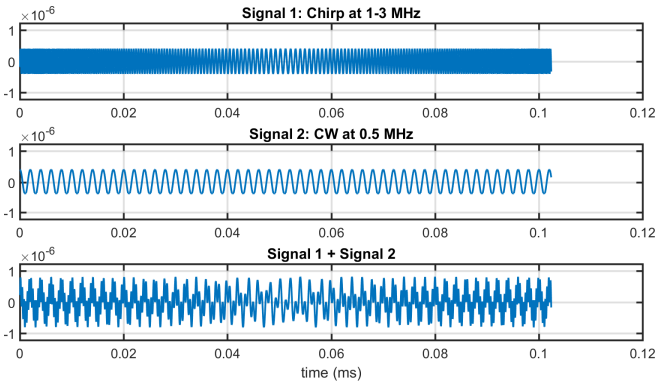

Fig. 1. Chirp + CW example signal.

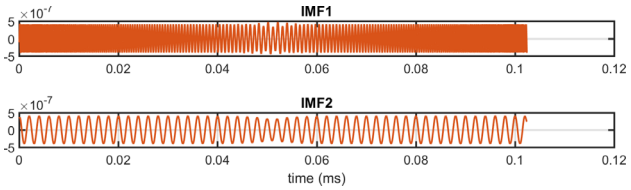

Fig. 2. Resulting IMFs after EMD decomposition of Fig. 1 signal.

components, discarding those containing noise. If the EMD signal decomposition is sparse in relation to the noise, then it would allow for efficient denoising. This basic idea can also be used for RFI filtering in passive microwave instruments.By adding up only the noise components, an estimation ofthe uncontaminated radiometric signal can be obtained. Given the useful properties that the EMD exhibits, especially local adaptability, it may be a good approach to working with nonstationary signals. EMD has been explored as an RFI mitigation strategy for active instruments [17], but to the authors' knowledge, no performance evaluation has been attempted for passive sensors. In Section III-A, a practical implementation of EMD for passive RFI mitigation is proposed, and the caveats and opportunities of this approach are analyzed. Another common RFI-mitigation technique, frequency blanking (FB), is used as a comparison benchmark to put EMD results into context.

A. Classical EMD Thresholding

Different criteria to quantitatively determine the presence of signal components have been developed. In particular, it has been pointed out that, in the presence of Gaussian noise, the EMD is approximately equivalent to a dyadic filter bank [18], [19]. In other words, the higher-order IMFs can be interpreted as the result of overlapping bandpass filters of the input signal. The first IMF is approximately the result of a half- band high-pass filter, and each IMF of higher-order contains frequency components that are roughly in the upper half-band of the previous IMF [20]. Following this interpretation, it can be deduced that, in the sole presence of noise and because the bandwidth is halved, the variance of the IMFs decreases geometrically with the IMF order by a factor of ≈2 in

TABLE I

VALUES FOR α AND β TO ACHIEVE DIFFERENT P_{fa}

	95%	99%
α	0.474	0.460
β	-2.449	-1.919

each iteration. According to [19], the variance of the IMF component of order k can be approximated by the following expression, which depends on the variance of the first IMF:

$$\sigma_k^2 = \frac{\sigma_1^2}{0.719} \cdot 2.01^{-k}. \quad (3)$$

A threshold can be defined above this model. To do that,a probability of false alarm (P_{fa}) has to be defined. For example, the 99% confidence interval (and therefore that achieves a $P_{fa} = 1\%$) c

$$th_k^{99\%} = \sigma_k^2 + 2^{\alpha \cdot k + \beta} \quad (4)$$

where $\alpha = 0.46$ and $\beta = -1.919$. Therefore, if an IMF of variance σ_k^2

$$\sigma_k^2 > th_k^{99\%}, \quad (5)$$

it can be considered unwanted signal components or RFI and can be discarded as such. Numerical values for 95% confidence thresholds can be found tabulated at [19] and are reproduced here for the sake of completeness (Table I).

Let us consider first the case where the RFI is confined in the lower part of the spectrum after frequency down-conversion. A simulated Gaussian noise signal of 300 K of power and 20 MHz of bandwidth has been combined with a sinusoidal waveform of 600 K of power and 1 MHz of frequency, simulating contamination by RFI. The combined signal is shown in Fig. 3, and the resulting decomposition in Fig. 4.

In this case, when compared to the noise, the RFI is "low frequency," it is safe to assume that the first IMF will be RFI-free, and therefore the threshold derived from the variance of the first IMF can be safely applied. In Fig. 5, the variances for each IMF component are plotted. In addition, the confidence interval (4) has been illustrated. As it can be appreciated in Fig. 4, the RFI is clearly detected in IMF 5, where the sinusoidal component can easily be identified. The comparison with the threshold in Fig. 5 makes it possible to identify also IMF 6 as containing a significant RFI contribution. The RFI-filtered signal can be then computed as the sum of all the IMF components except components 5 and 6.

There are some further important points to consider as follows.

1) Any discarded component contains a nonnegligible fraction of the radiometric noise and, as a consequence, the RFI-filtered signal power will be systematically biased. This power loss has to be accounted for and properly compensated, for which a model of the noise power of each component must be available. In this case, the modeled power given by (3) can be used for this purpose. When the components are uncorrelated (e.g., frequency binning, time binning, etc.), it suffices to add up the modeled power of the discarded components. EMD is, however, a decomposition whose components are correlated, and therefore the cross-variances must be taken into consideration as well.

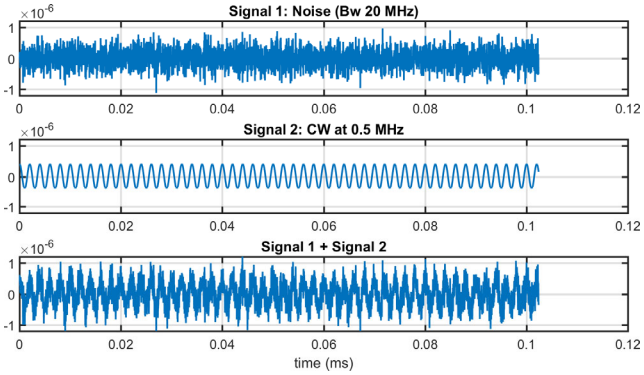

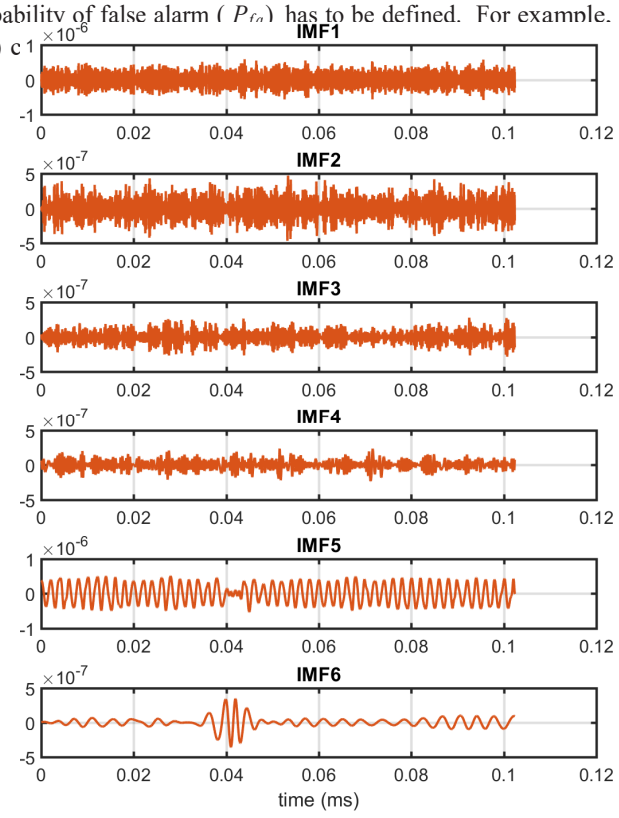

Fig. 4. Resulting EMD decomposition (first six IMF components) from the signal of Fig. 3.

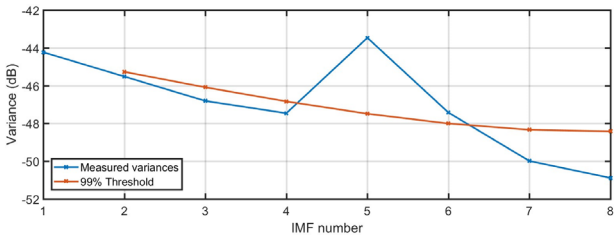

Fig. 5. IMFs variances in $\log_2$, along with the 99% confidence thresholds (red line).

2) Some fractions of the RFI may be contained in components considered RFI-free, and therefore their power will not be mitigated.
3) The resulting mitigated power will be of the lower radiometric resolution, and this will depend on the fraction of the noise power that is discarded.

These considerations are not specific to this method and can be found in other decomposition-based techniques such as time/frequency binning. The performance and limitations of this classic method will be studied and discussed in the following sections.

B. Multicomponent EMD Thresholding

The usefulness of this "low-frequency" RFI case is, however, very limited in a practical scenario. Note that this method is based on the strong assumption that the first IMF only contains noise samples. While this may be useful for removing slow-varying signals from a higher frequency noise, in the context of RFI mitigation, where the interference may appear at any frequency, this cannot be considered general. In fact,as shown in this work, RFI frequency must be under 1/4 of the noise bandwidth for the above condition to be true in a practical scenario (Fig. 12, and [20]). If this is not true, the power model of (3), and the thresholds of (4) will be higher than expected, and therefore no components will be detected as RFI. Therefore, to derive a practical RFI filtering technique from EMD a refinement to the above classical algorithm must be introduced.

The model for the IMF variances (3) can be written as a function of an arbitrary component, IMF_j. If this component is RFI-free, then it can be used as a reference, and an alternative threshold for the rest of IMFs can be computed as (from 4)

$$th_k^{99\%} = \sigma_j^2 \cdot 2.01^{j-k} + 2^{0.46 \cdot k - 1.919} \quad (6)$$

with $th_k^{99\%}$ denoting the threshold to be applied to IMF number k.

This alternative threshold computation still requires knowing beforehand which specific IMF component is free of RFI contamination, in order to be used as a reference. This requirement can be bypassed by running several parallel tests, each one assuming different IMF as RFI-free.

To exemplify this process, a hypothetical case of such parallel thresholding is shown in Figs. 6 and 7. In this exercise, the RFI is a combination of two continuous waves (CW): one is of low frequency (0.5 MHz) and another is of high frequency (12 MHz). By checking the measured variances of the IMF components in Fig. 6, it can be appreciated that the RFI appears as a deviation from the expected linear decreasing trend in IMF numbers 1 and 5, with possible spillovers of lower power in IMF 6. It should be noted how the contamination of the first IMF makes the use of classical EMD thresholding impossible.

In Fig. 7, the result of conducting nine parallel mitigation exercises is shown, each of them considering one different IMF as a candidate to be RFI-free (marked with green arrows). For each mitigation branch, the computed thresholds and model (6) are depicted. Any IMFs that are above the threshold have been identified with a red circle and would be removed for obtaining the mitigated power output. As it can be seen from Fig. 7, branch 1 is not able to detect the high-frequency component, and branch 5 is unable to detect any IMF as RFI contaminated. Branches #2, #3, #4, and #9 offer comparable results and are good candidates for proper mitigation of the majority of the RFI power, having detected the major RFI components and the spillover in IMF 6. Given that the removed power is conveniently compensated, the criteria to select the best branch could be the lowest power after mitigation.

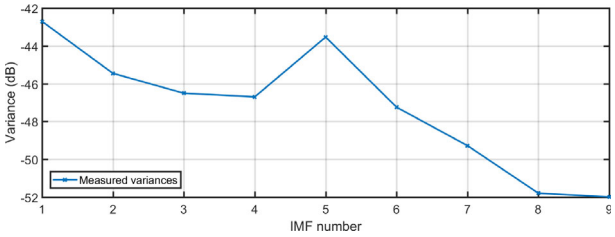

Fig. 6. IMFs measured variances in $\log_2$ for the multicomponent thresholding example of Fig. 7.

In summary, for the branches where the reference IMF is RFI-free, mitigation will work, and the resulting mitigated power will be close to the noise signal. In those cases where this assumption is not fulfilled, the resulting mitigated power will contain most of the RFI signal, and therefore the power will be higher. As a consequence, to identify the best option,it suffices to select the minimum mitigated power between the mitigation branches.[1] As it will be shown, this "multicomponent thresholding approach" allows for EMD to be used as an RFI detection method for high RFI frequencies as well.

It should be noted that this novel thresholding strategy is not limited to EMD, and it can be applied to any mitigation method where the threshold levels have to be estimated from the data themselves.

IV. Methodology

In order to evaluate the performance of the proposed methods, a simulated processing chain has been implemented. The radiometric signal (either the in-phase or in-quadrature components) has been simulated as a real random Gaussian process of 300 K of power with N 2^{14} independent samples. The combined signal is then passed through a digital anti-aliasing filter of B_W 20 MHz, and sampled at the Nyquist frequency Fs $2B_W$. This simulates the real low-pass equivalent of a generic radiometer signal.

In order to understand the behavior of EMD for the wide range of RFI signals, the performance is analyzed for the RFI signals described as follows.

1) *Delta function:* An instantaneous signal with all the RFI power concentrated in a single temporal bin.
2) *Amplitude-modulated CW:* A single tone signal (sinusoidal), simulating a narrowband modulation, of configurable frequency, and modulated with a slow-varying

[1] An additional check may be introduced in order to discard results whose radiometric resolution is too low.

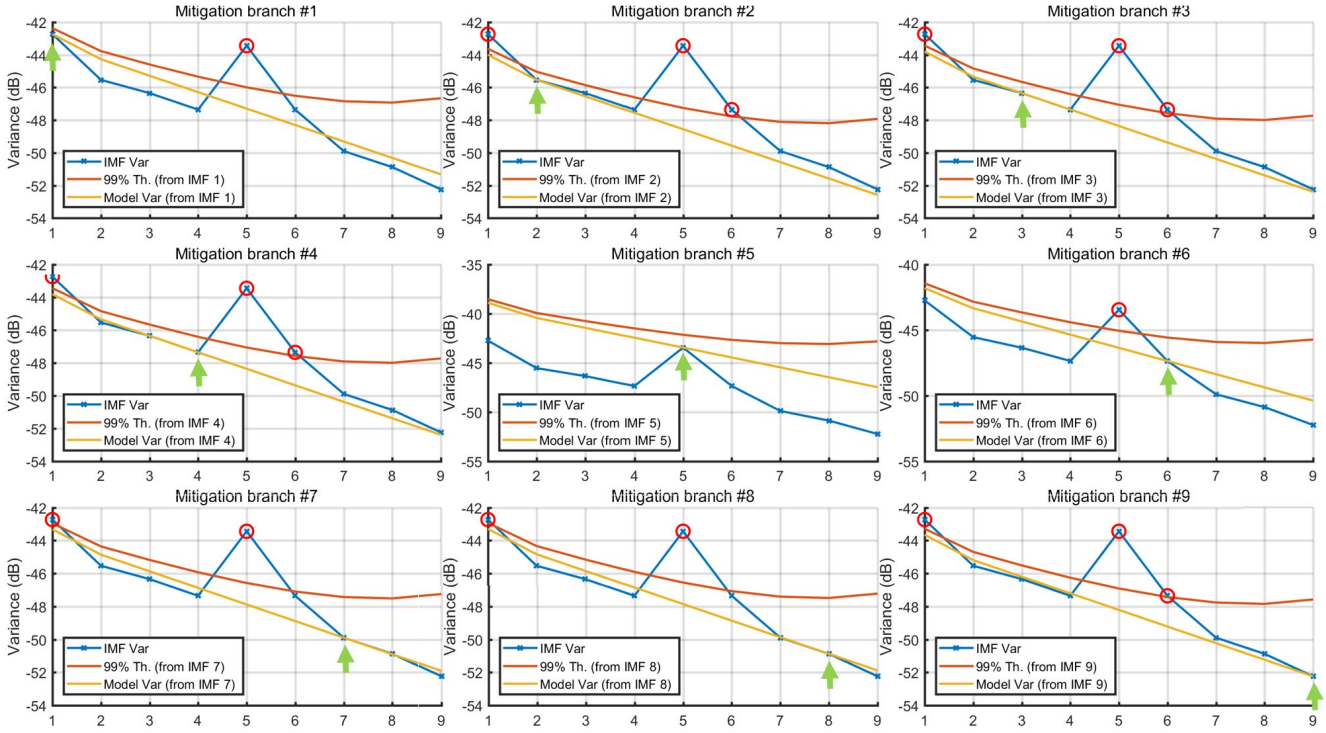

Fig. 7. Example of parallel multicomponent thresholding approach.

signal (resulting of the sum of two Gaussian envelopes) to make it nonstationary. This can represent, for example, a moving CW RFI source modulated by a Gaussian antenna pattern.

3) *Burst of pulses with a 10% duty cycle:* A train of rectangular pulses with a pulse repetition time (PRT) of $N/64$ samples, and a pulsewidth of PRT$/10$ samples. *Burst of pulses with a 50% duty cycle:* A train of rectangular pulses with a PRT of $N/64$ samples, a pulsewidth of PRT$/2$ samples, and configurable cen- tral frequency. Kurtosis detection exhibits a blindspot for this duty cycle and is therefore interesting to study how correlation-based RFI detection behaves in the same scenario.
4) *Narrow-band chirp signal:* A chirp signal sweepin linearly with an arbitrary bandwidth of $Bw/2$, and a PRT $N/16$ samples. Chirp signatures are representa- tive of RAdio Detecting And Ranging (RADAR) signals and jammers.
5) *Wide-band chirp signal:* A chirp signal sweeping linearly with an arbitrary bandwidth of Bw, and a PRT $N/16$ samples.
6) *Generic wide-band signal modulation:* Simulated using a pseudorandom noise code (PRN) of PRT N 16, with its nonuniform bandwidth overlapping the entire noise bandwidth.

Their spectrograms are presented in Fig. 8.

The combined signal is then decomposed using the EMD, and the presence of RFI is tested for each component. Decomposition is computed using the publicly available implementation of the EMD method [21] and with a maximum number of iterations $I_{\max}$ 25, and a maximum of 6 IMFs to guarantee a reasonable performance. Mitigation is then applied to the decomposed signal under the considerations discussed in Section III, and performance is assessed. To take into account the stochastic properties of RFI, NM 100 Montecarlo simulations have been executed for each scenario.

To have a reference to compare with, FB mitigation has been implemented as well. FB is based on the decomposition provided by the fast Fourier transformation (FFT). Each sample of the FFT of the contaminated signal is tested for RFI by comparison with a threshold, computed following [9, eq. 6]:

$$th_{FB} = 2\sigma_n^2 \ln\left(\frac{1}{P_{fa}}\right) \tag{7}$$

where σ_n^2 is the variance of the noise. The same probability of false alarm P_{fa} 1% than EMD has been chosen to compute the threshold. Note that, in a practical implementation of FB, σ_n^2 will also have to be estimated from the data themselves. To this effect, in this study, σ_n^2 is estimated by computing the median absolute deviation (MAD) of the ensemble [22]. The MAD is a robust estimator of the standard deviation of an ensemble in the presence of outliers and, as a consequence, its value will not be affected by the RFI as long as the number of affected frequency bins is low.

V. Results

A. Performance Evaluation

In this section, the mitigation performance achieved with the presented method is analyzed. Mitigation performance can be

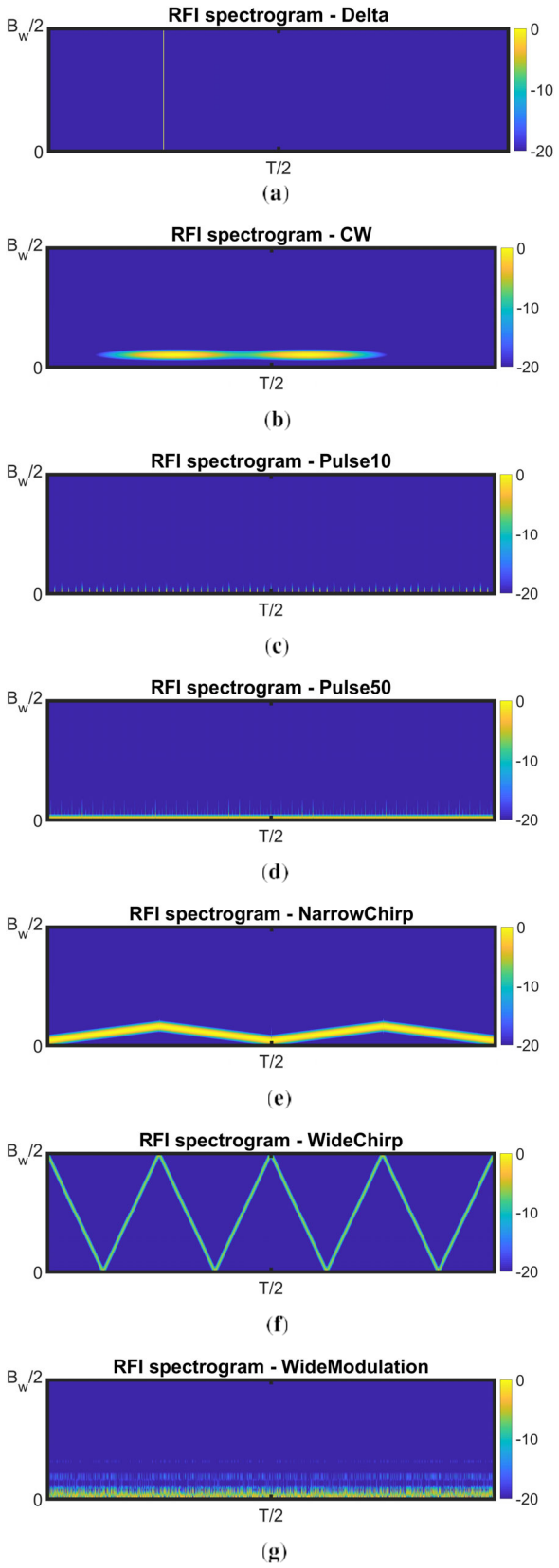

Fig. 8. Spectrograms of the different types of RFI considered in this study. (a) Delta function. (b) Amplitude modulated continuous wave. (c) Train of rectangular pulses (duty = 10%). (d) Train of rectangular pulses (duty = 50%). (e) Narrow-band chirp. (f) Wide-band chirp. (g) Wide-band modulation (PRN).

defined as the residual RFI power after mitigation, $\overline{T_b^{rfi}}$

$$\overline{T_b^{rfi}} = \overline{T_b^{n+rfi}} - T_b^n \quad (8)$$

where T_b^{n+rfi} is the resulting power after the mitigation process, and T_b^n is the brightness temperature of the radiometric noise. As a first step, the performance achieved will be analyzed for all RFI types by using the classical EMD thresholding. Specifically, for RFI signals with configurable central frequency (CW and narrowband and pulsed chirps), this is chosen to be 0.1 of the measurement bandwidth.In Fig. 9(a), the residual RFI power is plotted in function of the total input RFI power, T_b^{rfi}, for all the RFI types defined before.

From Fig. 9(a), it is clear that EMD is able to detect and mitigate most of the studied RFI types, as long as the RFI only contaminates partially the noise spectra. In the case of wide-band chirp or the delta RFIs, where the RFI overlaps the entire noise bandwidth, mitigation does not work. The EMDis not capable to untangle the chirp signal from the noise. All IMFs contain significant fractions of the chirp RFI and, as a consequence, no mitigation is possible.

In the presence of very impulsive signals, such as the delta function, it can be observed how the mitigation may result in higher residual power than the original signal. This is because EMD does not behave well with high-power impulsive signals, and the decomposition does not have any physical meaning. Due to the highly correlated character of mode-mixed components, removing some of them may lead to higher final RFI powers than the ones originally present. To account for that, additional filtering can be added to check if the signal power after mitigation is higher than the original power of the signal. If it is the case, it can be concluded that it was not possible to obtain a proper decomposition of the signal and then no mitigation should be attempted.

In Fig. 9(b), the performance results obtained with the FB are plotted as well. These results are well aligned with the equivalent results obtained in [9], and they will be used here as a reference. As it can be appreciated, FB is depending on the type of RFI. It works well for tonal RFIs, while it struggleswith chirps or wide-band signals [9].

A comparison between the EMD and the FB shows remarkable qualitative similarities. Both EMD and FB are well tailored for CW or narrow-band RFI. FB provides, however, better raw performance for most RFI types, especially in the case of CW and pulsed signals. Nevertheless, EMD provides better performance than FB for some selected types of RFI, especially narrow-band chirps and PRNs. This makes EMDa possible candidate for RFI mitigation in certain scenarios. In general, for those RFI types where mitigation is possible, EMD provides a similar level of mitigation regardless of RFI type, which makes it more balanced than FB.

In Section I, it has been mentioned that the EMD is a locally adaptive method, suitable to decompose nonstationary signals. Despite that, it is clear from the results presented that the EMD is not able to mitigate nonstationary signals overlapping the entire noise spectrum, such as wide-band chirp RFIs or Delta functions. The adaptiveness of EMD to the signal is not useful in the RFI mitigation scenario for passive instruments.

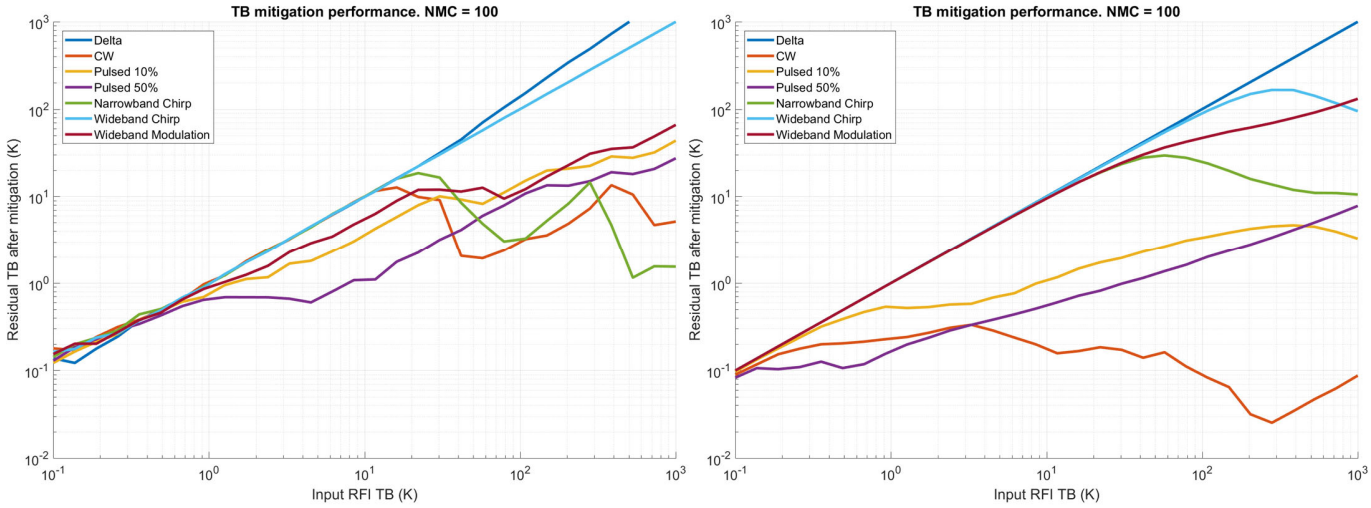

Fig. 9. RFI mitigation performance for the RFI types considered in this study. (a) EMD. (b) FB.

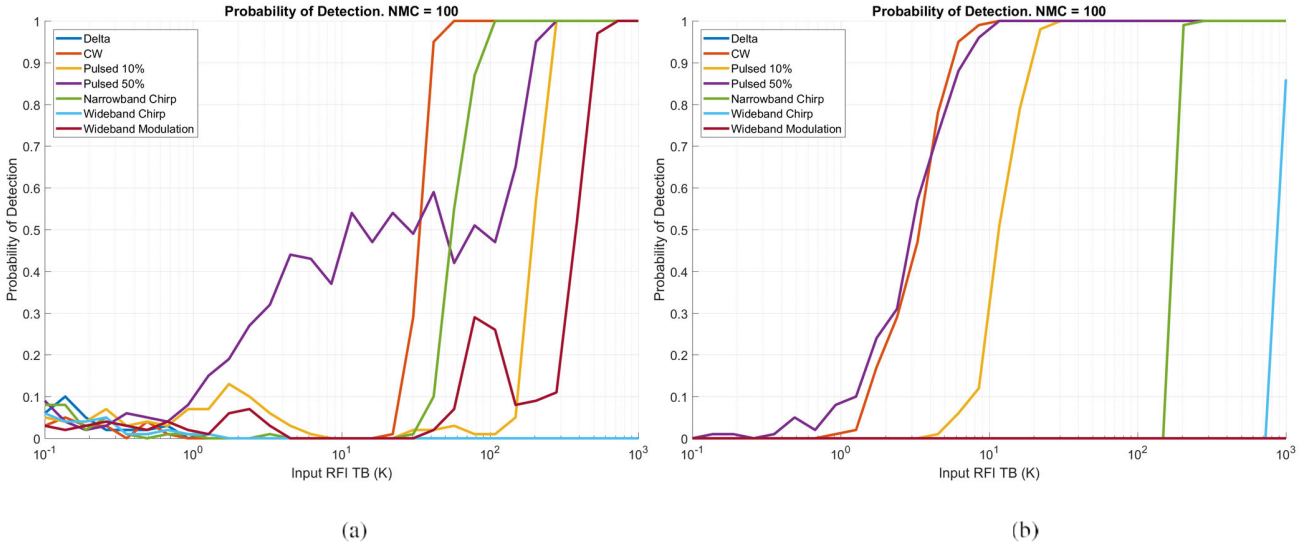

Fig. 10. PD for the RFI types considered in this study. (a) EMD. (b) FB.

This is because the method adapts to the highest frequency component present locally. In the presence of radiometric noise, the highest frequency component is the noise itself. Hence, the EMD behaves like a static dyadic filter, and no matching to the RFI occurs. This is an important caveat that advises against the use of EMD for passive instruments, as one of its most important properties cannot be exploited. The EMD performance is then qualitatively similar to those achieved with frequency binning, which again is reasonable if the dyadicfilter interpretation is followed.

In addition to the mitigation performance, the probability of detection (PD) can be computed. In this case, PD can be defined as the probability that the residual biases are below theRFI power. Specifically, if the residual is 0.1 of the RFI power,the RFI is considered detected and successfully mitigated (as 90% of its power has been removed). PD is then the number of "detections" divided by the number of simulation runs. Note that this definition of PD is different than the PD of each component [i.e., the probability to detect RFI in a given IMFs (EMD), or frequency bin (FB)].

In Fig. 10, the computed PDs are depicted. It is clear that frequency blanking is able to detect CW RFIs for lower RFI powers than EMD. Nevertheless, EMD exhibits earlier detection for narrow-band chirp and PRN signals. For some specific types of RFI, detection is not step-like; this is not fully understood, but it may be related to the nonlinearities present with EMD.

The last performance metric considered in this study is the resolution loss (RL). RL is defined as the fraction ofthe radiometric power that is eliminated from the signal after RFI mitigation. While this lost power can be compensated, this introduces an unavoidable degradation of the radiometric

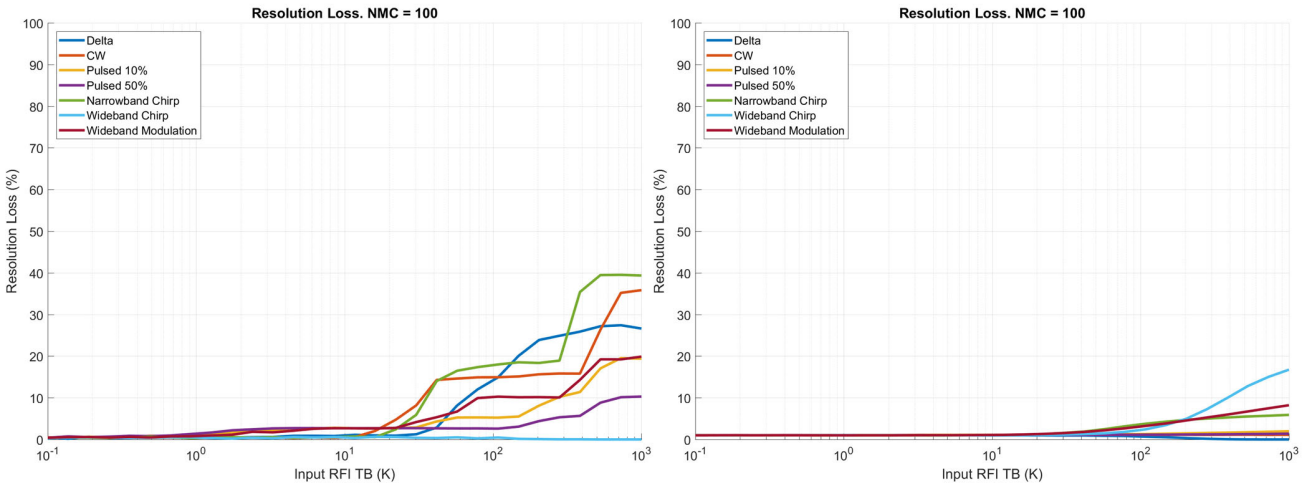

(a) (b)

Fig. 11. RL for the RFI types considered in this study. (a) EMD. (b) FB.

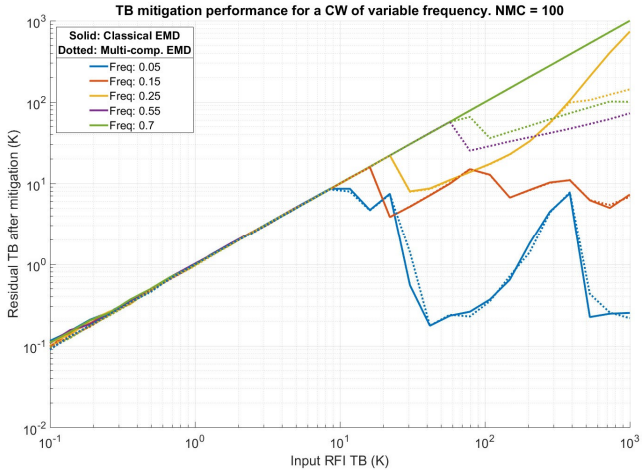

Fig. 12. Classical (solid) and multicomponent (dotted) EMD thresholding performance for a CW of variable frequency.

resolution (ΔT), and it is equivalent to a reduction of the integration time.

In Fig. 11, the RL results are plotted. RL is higher for EMD, something which is to be expected given the lower spectral resolution of EMD. It should be noted that RL in EMD is step-like. This is due to the limited number of IMFs that EMD produces, in contrast with the larger number of bins that FB has.

B. Dependence on RFI Signal Frequency

As a second step, the strong limitations presented by classical EMD thresholding are analyzed in this section, along with the results obtained with the refined thresholding presented in this work. Performance is analyzed for a CW RFI of variable frequency. First, detection is performed only by using the thresholds given by (4) (i.e., the classical EMD thresholding). In Fig. 12, the resulting mitigation performance is plotted in solid lines in function of the input interference power and for different CW frequencies.

As it can be appreciated, this method achieves a reasonably good performance while the CW frequency is below $Bw/4$. If the RFI frequency is higher than this value, the first IMF is contaminated, the RFI is undetected, and it cannot be mitigated and, as a consequence, the performance curve appears close to the unitary-slope line. This demonstrates that the single-threshold EMD classical technique is impractical for the mitigation of high-frequency RFI.

Let us analyze now the results with the multicomponent EMD thresholding approach. In Fig. 12, the resulting mitigation performance for this case is also plotted in dotted lines in function of the input interference power. With this strategy, mitigation is able to work successfully also at higher frequencies. Performance is, however, degraded when considering high-frequency RFI, something that is clear by considering the nonnegligible residuals, which increase with frequency. This can be understood by examining the dyadic filter interpretation of EMD, with the lower-order IMFs, containing the higher frequencies, being wider and therefore less capable of discriminating RFI.

Its marked dependence on RFI frequency makes the adoption of this method hardly justifiable in a general case, especially if the added implementation complexity is factored in. However, the EMD may still be an alternative in selected scenarios. In a low-frequency RFI environment, for example, EMD performs better than FB for some types of RFI, and it is in general a balanced approach for most types of RFIs. The use of EMD is well-tailored for RFI affecting the lower part of the measurement bandwidth, where the computation of the threshold is simpler, and where the spectral resolution of the method is best. It is not, however, a technique that enables better detection of nonstationary signals in the passivescenario: as mentioned, in that regard, FB and EMD are similar.

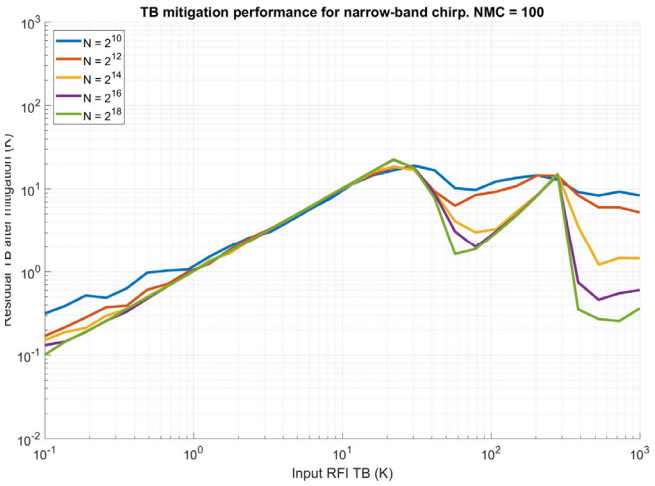

Fig. 13. Mitigation performance for narrow-band chirp for different sample sizes.

C. Dependence on Sequence Length

The prior analysis has been conducted with $N = 2^{14}$ samples, which assuming a sampling frequency of 40 MHz equals a sequence length of around 41 ms. In order to understand how the EMD performance changes with sequence length, the analysis has also been conducted with other reasonable numbers for N. Without loss of generality, mitigation performance achieved has been computed for the narrow-band chirp RFI type, and it is depicted in Fig. 13.

As it can be appreciated, the EMD is able to work with comparable performance for a wide range of sequence lengths. Lower sequence lengths exhibit a poorer performance in the mitigation region, but mitigation levels are reasonably good for all sample sizes considered.

VI. Conclusion

In this work, the possibilities of using the EMD as an RFI-filtering method for passive radiometry are studied. It hasbeen shown that the application of the classical thresholding strategy is not useful for RFI filtering due to the strong constraints on the RFI frequency. The usual strategy for EMD denoising is based on the assumption that the first IMF only contains noise. If this holds, a variance model for the rest of the IMF noise components can be derived, and therefore, the presence of RFI can be tested by comparison with a threshold.It has been shown that for RFI mitigation, this only works when the RFI frequency components are $< B_W/4$.

In order to overcome this, a refined approach is proposed in this work. The noise model and thresholds are derived from each IMF component separately, and each model is then used in a separate detection branch. Once the mitigated powers for each branch are obtained, the minimum of the ensemble is selected, as is the one that minimizes the residual power. This multicomponent model strategy has the potential to be applied to other decomposition schemes as well, especially when a data-derived noise model is required. In addition, the EMD has some novel challenges that have been addressed: since the IMFs are correlated, their covariance matrix has to be taken into account to compensate for the radiometric power lost during mitigation.

The performance achieved by the EMD is studied by computing three different performance metrics: mitigation residuals, PD, and RL. Performance is then compared with FB. It has been found that their behavior is qualitatively similar, with FB working better for CW RFI, and EMD for narrow-band chirps. However, it has been concluded that EMD is not showing adaptiveness to nonstationary RFI. The rationale is that the EMD adapts locally to the "highest frequency available" and, in the case of microwave radiometry, this is always found in the noise component.

EMD works reasonably well for RFI affecting the lower part of the measurement bandwidth, where the computation of the threshold is direct, and where the spectral resolution of the method is the best. In this scenario, EMD is an interesting alternative to other commonly applied methods, offering good performance for some types of RFI. However, in a general case, the complexity of EMD and its limitations may still be a problem.

This analysis is an important first step in the exploration of nonlinear decomposition methods for RFI mitigation. We consider that the potential that these types of decomposition schemes are enormous, especially when treating nonstationary signals. As mentioned, many variations of EMD have been developed to mitigate some of their problems, such as EEMD or adaptive local iterative filtering (ALIF). These improved techniques are worth to be assessed in the context of RFI mitigation as well. In addition, other nonlinear transformations are also worth trying. In this context, some of the challenges encountered in this work can be applied there as well.

References

[1] S. Misra and P. de Matthaeis, "Passive remote sensing and radio frequency interference (RFI): An overview of spectrum allocations and RFI management algorithms," *IEEE Geosci. Remote Sens. Mag.*, vol. 2, no. 2, pp. 68–73, Jun. 2014.

[2] D. W. Draper, "Radio frequency environment for Earth-observing passive microwave imagers," *IEEE J. Sel. Topics Appl. Earth Observ. Remote Sens.*, vol. 11, no. 6, pp. 1913–1922, Jun. 2018.

[3] National Research Council, *Spectrum Management for Science in the 21st Century*. Washington, DC, USA: The National Academies Press, 2010.

[4] D. Borio, C. O'Driscoll, and J. Fortuny, "Tracking and mitigating a jamming signal with an adaptive notch filter," Inside GNSS, vol. 9, pp. 67–73, 2014.

[5] S. Misra, P. N. Mohammed, B. Guner, C. Ruf, J. R. Piepmeier, and J. T. Johnson, "Microwave radiometer radio-frequency interference detection algorithms: A comparative study," *IEEE Trans. Geosci. Remote Sens.*, vol. 47, no. 11, pp. 3742–3754, Nov. 2009.

[6] T. W. Anderson and D. A. Darling, "A test of goodness of fit," *J. Amer. Stat. Assoc.*, vol. 49, no. 268, pp. 765–769, 1954.

[7] R. Díez-García and A. Camps, "A novel RFI detection method for microwave radiometers using multilag correlators," *IEEE Trans. Geosci. Remote Sens.*, vol. 60, pp. 1–12, 2022.

[8] A. Camps *et al.*, "Radio-frequency interference detection and mitigation algorithms for synthetic aperture radiometers," *Algorithms*, vol. 4, no. 3, pp. 155–182, 2011.

[9] J. Querol, R. Onrubia, A. Alonso-Arroyo, D. Pascual, H. Park, and A. Camps, "Performance assessment of time-frequency RFI mitigation techniques in microwave radiometry," *IEEE J. Sel. Topics Appl. Earth Observ. Remote Sens.*, vol. 10, no. 7, pp. 1–11, Feb. 2017.

[10] M. A. Colominas, G. Schlotthauer, and M. E. Torres, "Improved complete ensemble EMD: A suitable tool for biomedical signal processing," *Biomed. Signal Process. Control*, vol. 14, pp. 19–29, Nov. 2014.
[11] J. Han and M. van der Baan, "Empirical mode decomposition for seismic time-frequency analysis," *Geophysics*, vol. 78, no. 2, pp. O9–O19, Mar. 2013.
[12] Z. Liu *et al.*, "Application of empirical mode decomposition and artificial neural network for automatic bearing fault diagnosis based on vibration signals," *Appl. Acoust.*, vol. 89, no. 3, pp. 16–27, Mar. 2015.
[13] N. E. Huang *et al.*, "The empirical mode decomposition and the Hilbert spectrum for nonlinear and non-stationary time series analysis," *Proc. Roy. Soc. London A, Math., Phys. Eng. Sci.*, vol. 454, no. 1971, pp. 903–995, 1998.
[14] Y. Gao, G. Ge, Z. Sheng, and E. Sang, "Analysis and solution to the mode mixing phenomenon in EMD," in *Proc. CISP*, vol. 5, 2008,pp. 223–227.
[15] Z. Wu and N. E. Huang, "Ensemble empirical mode decomposition: A noise-assisted data analysis method," *Adv. Adapt. Data Anal.*, vol. 1, no. 1, pp. 1–41, 2009.
[16] H. Wu, "Current state of nonlinear-type time-frequency analysis and applications to high-frequency biomedical signals," *Current Opinion Syst. Biol.*, vol. 23, pp. 8–21, Oct. 2020.
[17] C. Yu, Y. Zhang, Z. Dong, and D. Liang, "Adaptive RFI suppression algorithm based on CEMD for SAR data," in *Proc. Int. Workshop Multi-Platform/Multi-Sensor Remote Sens. Mapping*, Jan. 2011, pp. 1–5.
[18] Z. Wu and N. E. Huang, "A study of the characteristics of white noise using the empirical mode decomposition method," *Proc. Roy. Soc. London A, Math., Phys. Eng. Sci.*, vol. 460, no. 2046, pp. 1597–1611, Jun. 2004.
[19] P. Flandrin, P. Gonçalves, and G. Rilling, "EMD equivalent filter banks, from interpretation to applications," in *Hilbert-Huang Transform and Its Applications*. Singapore: World Scientific, 2005, pp. 57–74.
[20] P. Flandrin, G. Rilling, and P. Goncalves, "Empirical mode decomposition as a filter bank," *IEEE Signal Process. Lett.*, vol. 11, no. 2, pp. 112–114, Feb. 2004.
[21] G. Rilling. (Nov. 17, 2021). *Empirical Mode Decomposition*. [Online]. Available: http://perso.ens-lyon.fr/patrick.flandrin/emd.html
[22] P. J. Rousseeuw and C. Croux, "Alternatives to the median absolute deviation," *J. Amer. Statist. Assoc.*, vol. 88, no. 424, pp. 1273–1283, Dec. 1993.

Raúl Díez-García (Graduate Student Member, IEEE) was born in Barcelona, Spain, in 1990. He received the M.S. degree in telecommuni- cations engineering from Universitat Politécnica de Catalunya (UPC), Barcelona, in 2014, where he is currently pursuing the Ph.D. degree in radio-frequency interference detection and mitiga- tion techniques with the Passive Remote Sens- ing Group, Department of Signal Theory and Communications.

In 2013, he was with European Space Agency (ESA-ESTEC), Noordwijk, The Netherlands. Since 2013, he has been working as an Earth Observation Engineer at ESA's Soil Moisture Ocean Salin- ity (SMOS) Satellite [ESA-European Space Astronomy Center (ESAC)], Madrid, Spain. His main research interests are in the area of microwave remotesensing and signal and image processing.

Adriano Camps (Fellow, IEEE) was born in Barcelona, Spain, in 1969. He received the M.S. degree in telecommunications engineering and the Ph.D. degree in telecommunications engineering from the Universitat Politécnica de Catalunya (UPC), Barcelona, in 1992 and 1996, respectively.

From 1991 to 1992, he was at the ENS des Télécommunications de Bretagne, Brest, France, with an Erasmus Fellowship. Since 1993, he has been with the Electromagnetics and Photonics Engineering Group, Department of Signal Theory and Communications, UPC, where he was an Assistant Professor, an Associate Professor in 1997, and a Full Professor since 2007. In 1999, he was on sabbatical leave at the Microwave Remote Sensing Laboratory, University of Massachusetts, Amherst, MA, USA. Since 1993, he has been deeply involved in the European Space Agency Soil Moisture Ocean Salinity (SMOS) Earth Explorer Mission, from the instrument and algorithmic points of view, performing field experiments, and since 2001 studying the use of Global Navigation Satellite System (GNSS)-R techniques to perform the sea-state correction needed to retrieve salinity from L-band radiometric observations. He has published over 216 articles in peer-reviewed journals, six book chapters, one book, and more than 450 international conference presentations,holds 12 patents, and has advised 23 Ph.D. thesis students (+ 8 on-going), and more than 140 final projects and M.Eng. theses. According to Publish or Perish (Google Scholar), his publications have received more than 7161/10 706 citations, and his H-index is 39/51 according to Scopus/Google Scholar. His research interests are focused on microwave remote sensing, with special emphasis on microwave radiometry by aperture synthesis techniques, remote- sensing using signals of opportunity (GNSS-R), radio-frequency detection and mitigation techniques for microwave radiometry and GNSS, and CubeSats as platforms to test novel remote-sensing concepts.

Dr. Camps received several awards, including the EURopean Young Investigator (EURYI) Award in 2004, the Duran Farell Award for technology transfer in 2000 and 2010, and the Institució Catalana de Recerca i Estudis Avançats (ICREA) Acadèmia Research Award in 2014. He was the IEEE Geoscience and Remote Sensing Society (GRSS) President from 2017 to 2018, the Technical Program Committee Chair of the International Geoscience and Remote Sensing Symposium (IGARSS) in 2017, the General Co-Chair of IGARSS in 2020, and he has been involved in the organization of several other conferences.

Hyuk Park (Senior Member, IEEE) was born in South Korea. He received the B.S. degree in mechanical engineering from the Korea Advanced Institute of Science and Technology (KAIST), Daejeon, South Korea, in 2001, and the M.S. and Ph.D. degrees in information and mechatronics from the Gwangju Institute of Science and Technology (GIST), Gwangju, South Korea, in 2003 and 2009, respectively.

In 2009, he joined the Remote Sensing Group, Polytechnic University of Catalonia (UPC), Barcelona, Spain, as a Post-Doctoral Researcher. In 2011, he was a grant holder of the National Research Foundation funded by the Korean Government. Since 2012, he has been working as a Research Associate witha Juan de la Cierva grant funded by the Spanish Ministry of Economy and Competitiveness. He is currently working with the Castelldefels School of Telecommunications and Aerospace Engineering (EETAC-UPC), Barcelona, as a Ramon y Cajal Fellow/tenure-track Assistant Professor. He is also working with the Passive Remote Sensing Group, UPC, for satellite remote sensing for microwave radiometry and Global Navigation Satellite Systems reflectometry. His main research interest is in the area of remote sensing, particularly passive microwave remote sensing, including system design, modeling and simulation, image/data processing, and small satellite applications.

Dr. Park is the winner of the Chong-Hoon Cho Academic Award, South Korea, in 2019.